Chemical Vapor Deposition

DOI: 10.1002/cvde.200506452

Full Paper

Evolution of the Field-Emission Properties of Individual Multiwalled Carbon Nanotubes Submitted to Temperature and Field Treatments

By *Stephen T. Purcell,* Pascal Vincent, Monica Rodriguez, Catherine Journet, Stephane Vignoli, Dominique Guillot,* and *Anthony Ayari*

Field-emission (FE) electron and ion microscopies (FEM and FIM), $I(V)$ characteristics, and FE energy spectroscopy (FEES) measurements have been made on individual multiwalled carbon nanotubes (MWNTs) at various stages of their evolution under various thermal and field treatments. Before the highest temperature treatments, the FE is produced by nanometer-scale structures that have specific and known characteristics such as individual peaks in the total energy distributions (TEDs), highly curved Fowler–Nordheim (FN) plots, and strong local heating due to the Nottingham effect. After cleaning at up to 1600 K, the TEDs approached the well-known form for FN tunneling from a free electron gas. As previously reported, they revealed and quantified strong heating at high FE currents induced by Joule heating along the MWNT. The TEDs gave a quantitative simultaneous measure of the temperature at the end of the MWNT, T_A (which reached up to 2000 K), and its electrical resistance R, thus allowing the determination of $R(T_A)$. $R(T_A)$ decreased by ca. 70 % as T_A increased from 300 to 2000 K, indicating a nonmetallic behavior of the MWNT. Changes in the MWNT length due to the induced high temperatures above 1600 K could be followed using the $I(V)$ characteristics. The high temperatures were accompanied by light emission due to incandescence for which the optical spectra was found to follow the Planck distribution. With the simultaneous measurements of T_A and R, the 1D heating problem could be reliably simulated to estimate the dependence of both electrical and thermal conductivities on temperature. This heating results in an excellent current stability by continuous desorption, and defines the maximum nanotube currents for high-current applications

Keywords: Adsorbates, Electrical conductivity, Field emission, Nanotubes, Thermal conductivity

1. Introduction

The use of carbon nanotubes (CNTs) as field-emission (FE) electron sources[1–3] is the basis of many of the closest-to-market applications for CNTs. The identified applications, for which many prototypes have been demonstrated, include flat-panel displays,[4–7] lighting elements,[8,9] high-brightness electron microscopy sources,[10,11] microcathodes for parallel electron lithography and microscopy,[12,13] RF amplifiers,[14] portable X-ray systems,[15] gas discharge tubes,[16] and ionization vacuum gauges.[17] In general, these devices depend on the intrinsic CNT advantages of structural and chemical stability, high current carrying capacity, high aspect ratio, and low-cost mass production to permit extracting both stable and large FE currents.[18] To push these devices to their full potential, in-depth FE characterization studies must be carried out on the dependence of emission current on voltage, temperature, energy, time, and the CNT surface and bulk physical properties. Within this topic we discuss here a rather extensive set of FE experiments on MWNTs using most of the standard FE techniques.

A considerable body of FE studies now exist in the literature, including several extensive articles[19,20] and reviews,[21,22] with measurements on many aspects of FE from ensembles and individual CNTs of varying structural perfection, apex cleanliness, and degree of ex situ characterization. The results showed a wide spectrum of behavior, particularly in the few years following the first FE experiments of 1995. As examples, the $I(V)$ characteristics may, more or less, follow the FN law,[19,20,23] or tend either to bend up or to saturate at high currents.[24] FE microscopy (FEM) may show complicated emission patterns,[25,26] or those that come from well-specified closed CNTs whose apexes approach ideal structures.[27] The total energy distributions (TEDs) may show very narrow energy spreads[19,26] and multiple peaks,[26,28] or be those that approach standard theory.[29,30]

[*] Dr. S. T. Purcell, Prof. P. Vincent, M. Rodriguez, Prof. C. Journet, Prof. S. Vignoli, D. Guillot, Dr. A. Ayari
Laboratoire de Physique de la Matière Condensée et Nanostructures
Université Lyon 1; CNRS, UMR 5586
Domaine Scientifique de la Doua, 69622 Villeurbanne cedex (France)
E-mail: stephen.purcell@lpmcn.univ-lyon1.fr

The community may have been looking for something new in FE specifically related to the novel crystalline or electronic structure of CNTs; however, views are now converging to the idea that the $I(V)$ curves and TEDs from properly cleaned MWNTs are governed to first order by the FN theory. The very strong measured FE effects are not specific to CNT electronic structure but to a variety of secondary effects, particularly: 1) nanometer-scale adsorbate-like structures on the emitter zones; 2) emitter evolution during $I(V)$ measurements; 3) temperature increases during $I(V)$ measurements; and 4) contact resistances. These effects can be found in FE from many emitter systems. In addition to addressing these issues, our own group has particularly concentrated on high current behavior. FEM, FIM, and particularly FEES[31,32] measurements of the TEDs have been used to characterize individual MWNTs. FEES leads more directly to an understanding of the FE behavior. Studies have been carried out at various stages of the thermal and field cleaning of MWNTs. Notably, MWNTs cleaned at up to 1600 K[33] have been studied in order to: 1) measure the temperature at the apex emission zone, T_A, as a function of emission current I_{FE}; 2) prove that the FE current can induce high stable temperatures reaching 2000 K by Joule heating; 3) measure the electrical resistance of the individual MWNTs; 4) show that the high temperatures are accompanied by light emission from the MWNTs; 5) show that the high induced temperatures can lead to excellent emission stability by cleaning the surfaces of the nanotubes; and 6) show that even higher currents leads to a gradual destruction of the nanotubes. These studies were accompanied by simulations of the associated Joule heating and thermal transport problem that confirmed the main interpretations of the experimental data.[34]

In this article a much wider report of this work is given, including systematic FE measurements as the emitter evolves between the two regimes of before and after the highest temperature cleaning. The first regime is when the surface is rough and consists of disordered nanostructures formed either by adsorbates or the carbon itself. It is useful to give an account of these characteristics because: 1) it is certainly the most often encountered in MWNTs used in actual device applications where heating to 1600 K is not possible; 2) it explains many of the artifact effects found for FE measurements of MWNTs; and 3) it allows direct contrasts to be made with measurements of the clean state particularly for heat generation during FE. The second regime is when the surface has been heated to temperatures reaching 1600 K to produce a "smoother-cleaner" surface without nanometer-sized protrusions, and FE that follows roughly the FN theory. In addition to being the "intrinsic MWNT emitter", it will be shown how FE then becomes a versatile tool for making simultaneous and therefore correlated measurements of several CNT physical properties.

2. Results

The general experimental procedure is detailed in Section 5. This procedure generated an enormous amount of data especially because the measurement cycles caused tip changes themselves due to adsorption, and field- and temperature-induced surface diffusion. Only the essential points will be discussed.

2.1. Disordered Nanostructure Cap Regime

The first FEM patterns observed consist of a single spot with first emission voltage at around 300 V for ca. 1 pA obviously due to the emission from a field-induced adsorbate nanostructure on a single MWNT. This is generally what occurs for the first FE from any uncleaned tip. This emission was very unstable and often consisted of patterns (see Fig. 1a) similar to those observed in the original Muller experiments[35] on deposited molecules, and by Becker[36] for absorbed oxygen layers submitted to a field. This phenomenon has been recently re-interpreted theoretically by Sekatskii and Letokhov.[37] Such patterns have also been regularly observed for FE from uncleaned or lightly heated SWNTs and MWNTs,[19,28,26] and obviously are not specific to the intrinsic properties of CNTs, especially in the light of patterns with a clear correlation with expected MWNT structure.[27] These objects give rise to strong effects in the TEDs exactly as those measured from deposited molecules[38] that are a guide for emission from any such nanostructure. The resonant tunneling model[39] has been often invoked[31,38] to explain most of the effects (see below).

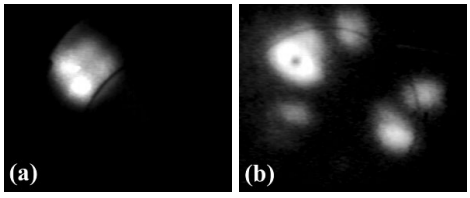

Fig. 1. a) FEM image of a pattern from a nanostructure formed by the action of field on the MWNT adsorbate layer. b) FEM image from the MWNT opened by field evaporation. The circular arrangement of spots corresponds to nanostructures distributed around the end of the open MWNT.

After heating cycles that went up to 1300 K, the emission became rather stable for currents in the nA range, and the spot pattern widened but was still due to nanoprotrusions that gave no signature specific to the MWNTs. Such nanoprotrusions exist even on Spindt cathodes.[40] They can also be readily formed starting with the Muller-type patterns if currents above the 100 nA range are used to harden them, when they then can become relatively stable. The TEDs still show the same abnormal characteristics of FE from

nanostructures mentioned above, though to a lesser degree. This places serious doubts on interpreting measurements on MWNTs that were not cleaned to even higher temperatures as pertinent to intrinsic CNT emission.[19,20] Also, the nanostructures often re-form under a field for MWNTs that are not regularly cleaned because adsorption layers eventually accumulate in any vacuum. This has been used to form on-axis protrusions on W<111> tips with large extra peaks in the TEDs.[41]

Cycles of field desorption and evaporation were then used to attempt to clean the MWNT, and to have a representative pattern that could be correlated with an MWNT structure. The broadened one-spot type patterns persisted until field desorption voltages of 2.4 kV were used, or roughly eight times the electron FE voltage for ca. 1 pA current. The pattern then evolved suddenly to a ring of relatively confined spots due to the apex region of a single MWNT, opened by the field desorption (see Fig. 1b). Similar field desorption has been carried out by Saito et al.[42] who opened the cap of a high-quality, small-diameter MWNT revealing roughly circular patterns. At this point we could be sure that the extended pattern was still due to a single MWNT because, during various field cycles, the whole FEM or FIM patterns would suddenly shift on the screen as a single unit. Furthermore, a new technique was developed for distinguishing individual MWNTs in a FE pattern by exciting their natural mechanical resonances with an AC field.[43]

Cycles of FEES, FEM, and $I(V)$ measurements were carried out on the MWNT interspersed with more field desorption. The first emitting MWNT was gradually shortened by field desorption resulting in a gradual increase in the operating voltage by ca. 20 %, and eventually the appearance of a second nanotube to the side emitting roughly ten times less current. Despite the fact that clean carbon surfaces were exposed, the FEM still always gave spotty patterns distributed around the circle and TEDs are of the nanostructure type. Different FE measurements of the principal MWNT that were similar to those at all previous steps are shown here. They can be considered characteristic of what will occur for most MWNTs used in devices that have not been cleaned to even higher temperatures.

Figure 2a shows a series of FEES measurements as a function of applied voltage, with the corresponding FN plot in Figure 2c. The signatures of such TEDs are: 1) the spectra are composed of one or several peaks; 2) the individual peaks still more or less approach the asymmetric forms predicted by the standard theory; 3) the high energy sides still widen with temperature as in the standard theory,[44] while they vary little on the low energy sides as a function of field; 4) the peaks shift roughly linearly with field (or voltage), see Figure 2b. The field shifting is a strong identifying characteristic for this type of emission, and often results in new peaks "arriving" at the Fermi level as the voltage shifts the whole spectra to lower energy. Figure 2c shows the corresponding FN plot for the TEDs of Figure 2a. It is highly nonlinear with a kink as each new peak arrives at the Fermi level.

FN plots can be quite straight over several decades when the TED is composed of one field-shifted peak (see the lower curve in Fig. 2c), so a FN plot over a limited range as used by many groups is not a sufficient criterion to prove that the emission does not come from a nanostructure or other type of near-surface potential. In general, the researchers measuring FE from MWNTs and depending only on the $I(V)$ curves should note that Dyke and Dolan[45] measured FN behavior over 16 orders of magnitude to support the FN model for FE from a W tip. Relatively straight FN plots obtained over several orders of magnitude just reflect the obvious fact that, to first order, the triangular barrier is being bent down more or less linearly with the field.

One aspect that has a direct relationship to the heating effects discussed in the next section is that the high energy side can be fitted to give approximately the temperature as a function of current,[44] though it is not clear how to fit this experimental fact into the resonant tunneling model. Figure 2d shows the temperature as a function of emission current when the TED was composed of the one peak for which the straight FN plot was obtained in Figure 2c. The heating occurs at very low current, and can be attributed to Nottingham effects. Strong heating occurs for such low currents because each emitted electron adds a large energy to the emitter due to the large field-induced energy shifts (e.g., ca. 0.5 eV), and furthermore all this energy is deposited in the emitting nanostructure. The temperature follows a power law with exponent 0.43. Such a dependence is usually found for the adsorbate nanoprotrusions formed on metal tips,[46] with exponents in the range 0.4–0.5. The power law can probably be modeled for a point heat source in contact with a heat reservoir.

In the presence of resonant tunneling, the local heating and nanometer size of the emission zone means that atomic re-arrangements are frequent, and strongly affect the total current. Typical measurements for current stability are shown in Figure 3 on a log plot. The current is very stable in the 1 nA range, but by 100 nA it undergoes large abrupt jumps at about a one minute intervals as the nanostructure from which all the current is coming undergoes many temperature-activated atomic-scale modifications. Dean et al.[47] proposed that such local heating by the Nottingham effect could explain the increase in the $I_{FE}(V)$ curves above the FN line at high current. We argued previously[34] that this may be part of the problem but that the main heating effects are Joule heating along the nanotube length (see Sec. 2.2). An additional argument is that to explain the current increase by FN theory, the emission zone must reach 1600 K. The local heating in the presence of nanostructures affects the current stability at much lower temperatures

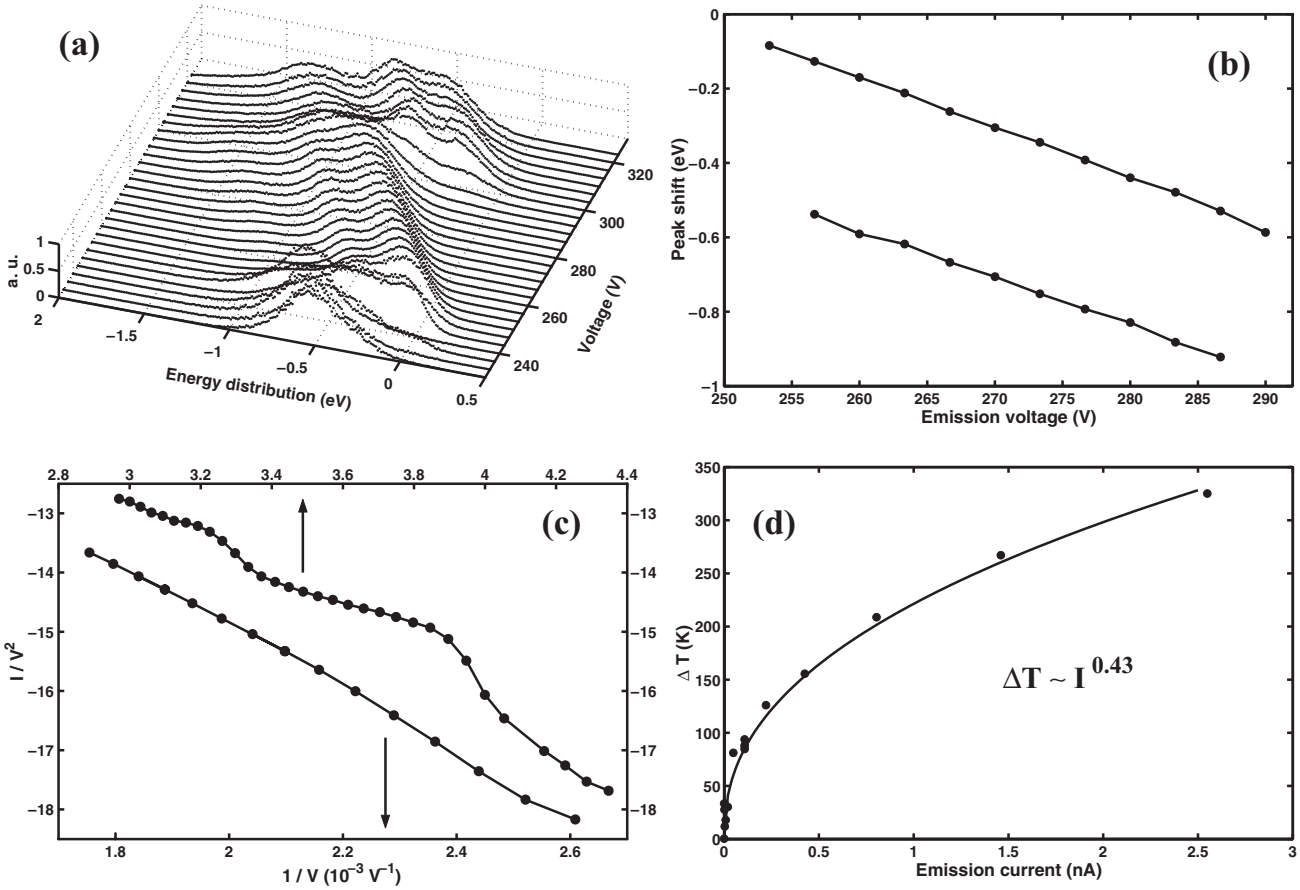

Fig. 2. a) Typical series of TEDs for the CNT after field desorption. b) Linear shifting with applied voltage of several of the peaks in (a). c) Corresponding FN plots. The upper curve is for the TEDs in (a). A kink occurs as each peak arrives at the Fermi level. The lower curve is for when only one field-shifting peak occurred in the TED. d) Temperature increase at the nanostructure found by fitting the TEDs when they consisted of only one peak (corresponding to the lower curve in (c)).

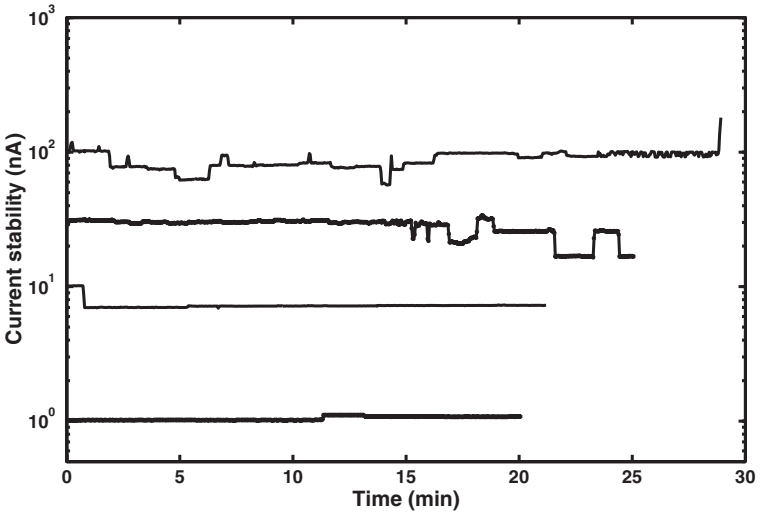

Fig. 3. FE current as a function of time for a MWNT emitting from a few nanostructures. The current becomes unstable above 1 nA.

(and currents) and does not permit enough stability to allow a measurement of an upswing in the FN plot at such high currents.

2.2. FE Studies after Heat Treatment to 1600 K

After the field evaporation cycles, the Ni tip holding the MWNTs was heated to the even higher temperature of 1600 K by electron bombardment. This changed most of the emission properties, with regard to FEM, $I(V)$, TEDs, and current stability. Some caution should be exercised with describing this treatment as a direct heating to 1600 K for two reasons. Firstly, the electron bombardment is actually done by attracting electrons emitted from another W loop by thermionic emission to the Ni tip held at +2 kV. Thus it was actually a combined field/heat treatment with the value of the field roughly four times that which would be necessary for the emission of electrons. Secondly, a temperature gradient may build up along the nanotube and thus the final temperature may be other than 1600 K. The MWNT could usually then be re-cleaned of the adsorbates and nanostructures that build up after exposure to the vacuum with a quick flash heating to only 1000–

1200 K, or by simply briefly emitting a current in the μA range (see below).

After the very first such electron bombardment treatment carried out for 10 min, the overall circle pattern (see Fig. 4a) and the extraction voltage was maintained, but the spots around the circle grew broader and started to present interference bands that have been previously observed in

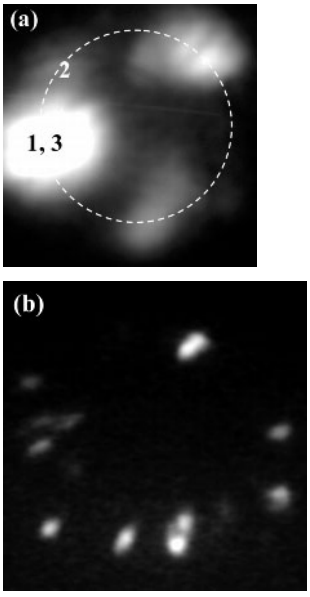

Fig. 4. a) FEM image of the MWNT after heating at 1600 K. b) FIM image of the MWNT cleaned to 1600 K made with Ar at 80 K.

much more dramatic detail[27] for high-quality, low-radius MWNTs. The fringes are attributed to interference of electrons coherently emitted from spatially separated zones on the MWNT apex.[48] These are not visible in Figure 4a, though they were often obvious on the video screen. These interference effects can be qualitatively differentiated from the previously mentioned Muller-type patterns. Here the interference occurred near the overlapping edges of emissions from adjacent emission zones and consisted of straight lines as in twin-slit interference.[48] In the case of the molecular structures, the whole emission spot is a diffraction pattern.

FIM patterns that confirm the open MWNT structure were taken at this point at 80 K with argon, and are composed of atomic sites distributed around the same circle as the FEM (see Fig. 4b). Unfortunately the contrast in FIM is so strong that only the very most protruding atoms were observed, similar to a constant height scanning tunneling microscope (STM) image. Also, using argon at 80 K does not give a very good FIM resolution to determine whether several atoms are represented by an individual spot. This makes it difficult to see the overall atomic-scale structure to confirm the improved crystallinity surrounding the protruding atoms and perhaps formation of pentagons and hexagons. Note that the selectivity for electron emission from protruding sites is much less than for ions because of the different nature of the tunneling barrier, and thus the TEDs are representative of larger surfaces.

Upon appearance of the interference bands, the resonant tunneling effects in the TEDs (i.e., the field shifting and existence of multiple peaks) disappeared, and the current became more stable even at higher currents well up to the microamp range. The TEDs were reproducible and approached the standard asymmetric peak from a metallic tip. A consistent picture can now be drawn that links the FEM patterns to the TEDs. The higher temperature heating permits crystallization at the MWNT apex that includes cross linking between different tube ends of the MWNT, smoothing of nanostructures, closing of dangling bonds, and thus elimination of local resonant tunneling states. The emitted electrons then come from the Fermi sea of the MWNT that have an internal coherence length that permits the formation of interference effects between different emission zones, as in a Young's slit experiment.[48]

Three series of TEDs were measured through the probe hole corresponding to the zones marked in Figure 4a. The TEDs were reproducible and approached the standard asymmetric peak expected from free electron theory. The formula for the TED of FE from a free electron gas $(J(E))$[31,49] is the product of a field-dependent transmission probability and the Fermi-Dirac distribution. Ignoring the energy independent pre-factors, it is given by Equation 1.

$$J(E) \propto \frac{\exp\left(\frac{E-E_F}{d}\right)}{1+\exp\left(\frac{E-E_F}{k_B T}\right)} \quad (1)$$

where k_B is the Boltzmann constant, T is the temperature, E_F is the Fermi energy, and $d \sim F_0/\sqrt{\phi} \sim 0.2$ eV. F_0 is the applied field (ca. 3–7 V nm^{-1}) and ϕ the work function in electronvolts. The TEDs are asymmetric peaks of width 0.3 eV at room temperature. The slope in the log plot is approximately $1/d$ on the low energy side, and ca. $(1/d–1/k_BT)$ $N–1/k_BT$ at 300 K on the high energy side. The peak is positioned close to E_F. In general the experimental measurements of TEDs from metallic emitters deviate to different degrees from this formula,[31] but they do permit an excellent measure of E_F and the temperature at the emission zone. We have found agreement within 20 K between optical pyrometry measurements and fits to Equation 1 in the range 1000–1300 K, and better than 0.05 eV for E_F for emission from W and Pt emitters in the same experimental setup.

TEDs from the brightest FE zone (Series 1) at various values of I_{FE} are shown in Figure 5a. First, the spectra at low voltage and current are considered. In agreement with previous work on clean MWNTs,[30] the form of the TEDs at low current and voltage are found to follow Equation 1 to first order. That is, the TEDs are composed of a single

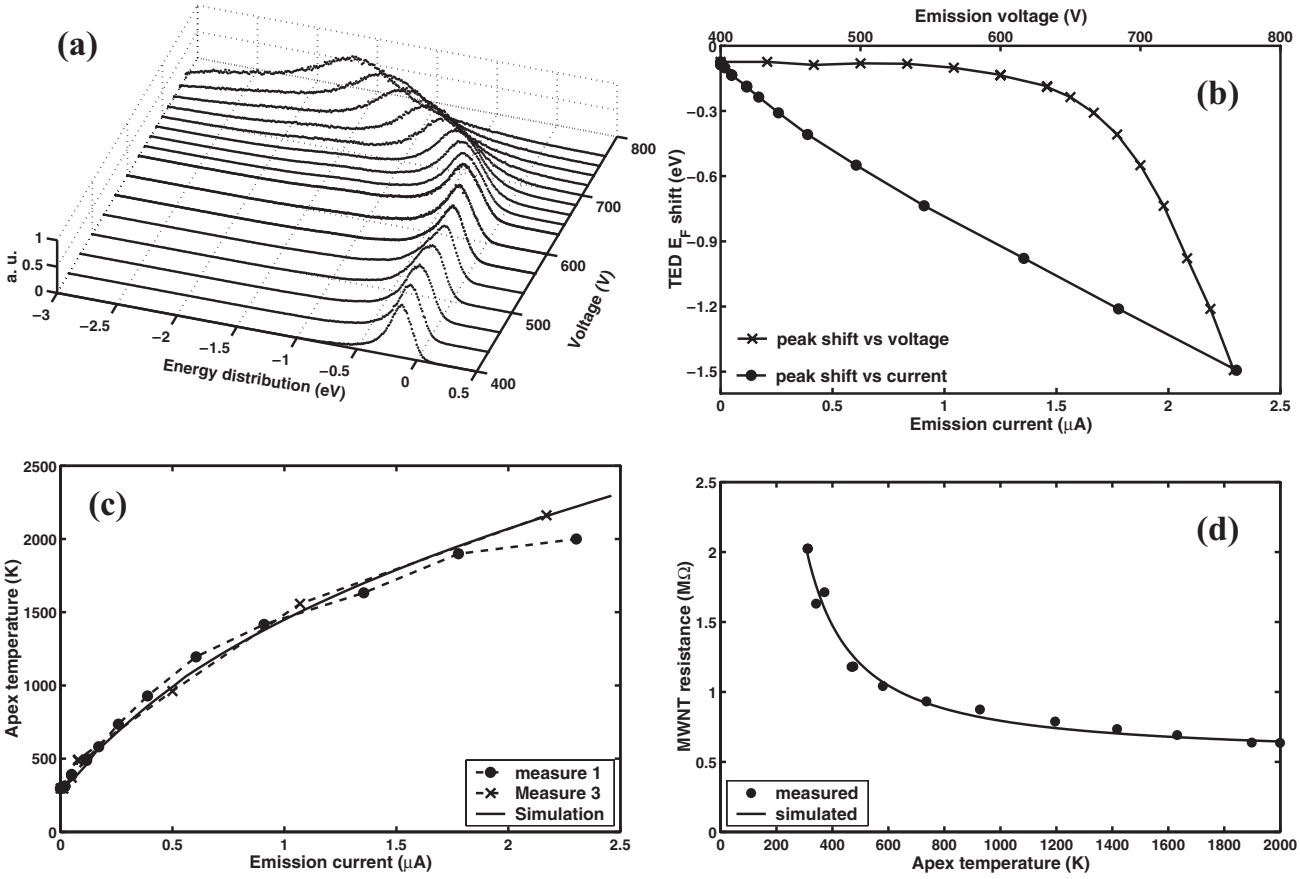

Fig. 5. a) Series of TEDs for the MWNT after electron bombardment heating to 1600 K. b) Shifting of the TEDs with current and voltage showing that the displacement is due to an IR drop and not a nanostructure. c) Temperature at the MWNT cap measured by fitting the TEDs for two runs. The solid line is a fit to the $T_A(I_{FE})$ curve using simulations of the heat equation (see Sec. 3). d) Total resistance of the MWNT as a function of apex temperature $R(T_A)$ for the TEDs in (a).

asymmetric peak fixed at E_F that widens principally on the low energy side as the increasing electric field increases the slope of the tunneling barrier. Looking more closely it is seen that: 1) there is a hump in the spectra at about 0.5–1.2 eV below the Fermi level similar to TEDs observed previously[30] on highly ordered MWNTs; 2) the fitted E_F is 70 meV below that expected for the voltage applied to the tip; 3) the temperatures found from the fitting are about 100 K higher than the true temperature of about 300 K; and 4) the full width at half maxima (FWHMs) are wider than usual for metal emitters. These second-order effects can be caused by the deviation of the electron density from that of a free electron model which is common even for clean metals.[31] (It has also been suggested that a larger than expected high-energy side is due to field penetration.[30]) From a practical point of view this sets a limit on the accuracy of the temperature measurement, particularly at low temperature. Much better agreement was found for W<111> FE tips in the same experimental configuration, and hence it is not due to a poor resolution of the energy analyzer. It is not obvious how to attribute the low energy hump to some specific feature in the density of states for carbon or nanotubes, even though it appears to be a common feature for several authors working with different types of MWNTs. Van Hove singularities should not be expected for such large MWNTs and the well known cusp for graphite layers is 2.7 eV below E_F, too far to be invoked.

At higher voltage and I_{FE}, the TEDs continued to widen on the low energy side as expected, but they displayed two new main characteristics. Firstly they shifted to lower energy due to a resistance drop along the MWNT, and secondly they also widened on the high energy side due to significant heating effects. The data was fitted to Equation 1 to extract the dependence of the parameters E_F, T_A, and d on the voltage and current.

In Figure 5b, the fits to the measured TEDs with Equation 1 for E_F against applied voltage and current are given, showing that E_F displaces to lower energy approximately linearly with I_{FE} (note that the I_{FE} axes in a previous report[33] should be multiplied by ca. 2). It is essential to not confuse this shift with the field-shifting of TEDs in the presence of the nanometric adsorbed structures shown above. In that case the shift is roughly linear in voltage, while here the shift is linear in I_{FE} and exponential in voltage. The obvious interpretation of this data is that the TED shifts because of a resistive IR drop along the MWNT. The shift gives resis-

tances in the megaohm range. As a direct consequence of these results, it is proposed that heating rises occur because of Joule heating along the MWNT. The existence of the heating of MWNTs to very high temperatures during FE for currents in the microamp range has also been proposed by Dean et al.[47] by interpreting the curving up of the FN plot and the FE patterns. The difference here is that it is Joule heating and not Nottingham effects that is proposed as the heating mechanism, and that the simultaneous direct measurement of temperature and resistance give the necessary inputs for modelization of the heat diffusion problem.[34]

In Figure 5c it is seen that T_A increased from 300 K (I_{FE} < 1 nA) to 2000 K (I_{FE} = 2.3 μA). The results for two runs on different sites are shown. A correction by quadrature was applied to the data for the offset at 300 K, but at 2000 K this correction accounts for only 20 K or 1 %. Errors at higher temperatures also occur because of humps that appear in the spectra on the high energy side as the spectra widen. From fitting various spectra variations are found of about 10 % over the whole temperature range. Note that the form of the $T_A(I_{FE})$ curves and the current scales are very different from those in Figure 2d (despite the fact that they were measured on the same MWNT) where the heating was attributed to local effects and were already appreciable at 1 nA.

The combination of independent measures of temperature and resistance enables a plot (Fig. 5d) of $R(T_A)$ defined as E_F/I_{FE}. This is plotted for two runs on the same MWNT. The resistance is in the megaohm range and decreases as T_A increases. This MWNT does not have metallic conductivity behavior. The total drop in resistance is ~70 % over the total temperature range. This measured dependence was recently used in simulations of the FE current induced breakdown of MWNTs.[50] Also shown is the fit to this data using the heat equation allowing for a variable electrical and thermal conductivity (see below).

There are at least three arguments that the measured resistance is due to the nanotube and not the contact at the Ni tip. Firstly, the CNTs were grown directly on bulk Ni and, other than the carbon, there are no semiconductor or oxides present so it is difficult to see how a contact resistance of several megaohms could exist. Secondly, the measured cap temperatures at 2000 K cannot be created by heating at the contact which would then have to be even hotter (greater than the melting point of Ni). Thirdly, the simulations are consistent with the measured apex temperatures and MWNT resistances.

In Figure 6a the parameter d and the FWHM are plotted against applied voltage for the different spectra measured. It can be seen in the figure that the fitted d and FWHM fol-

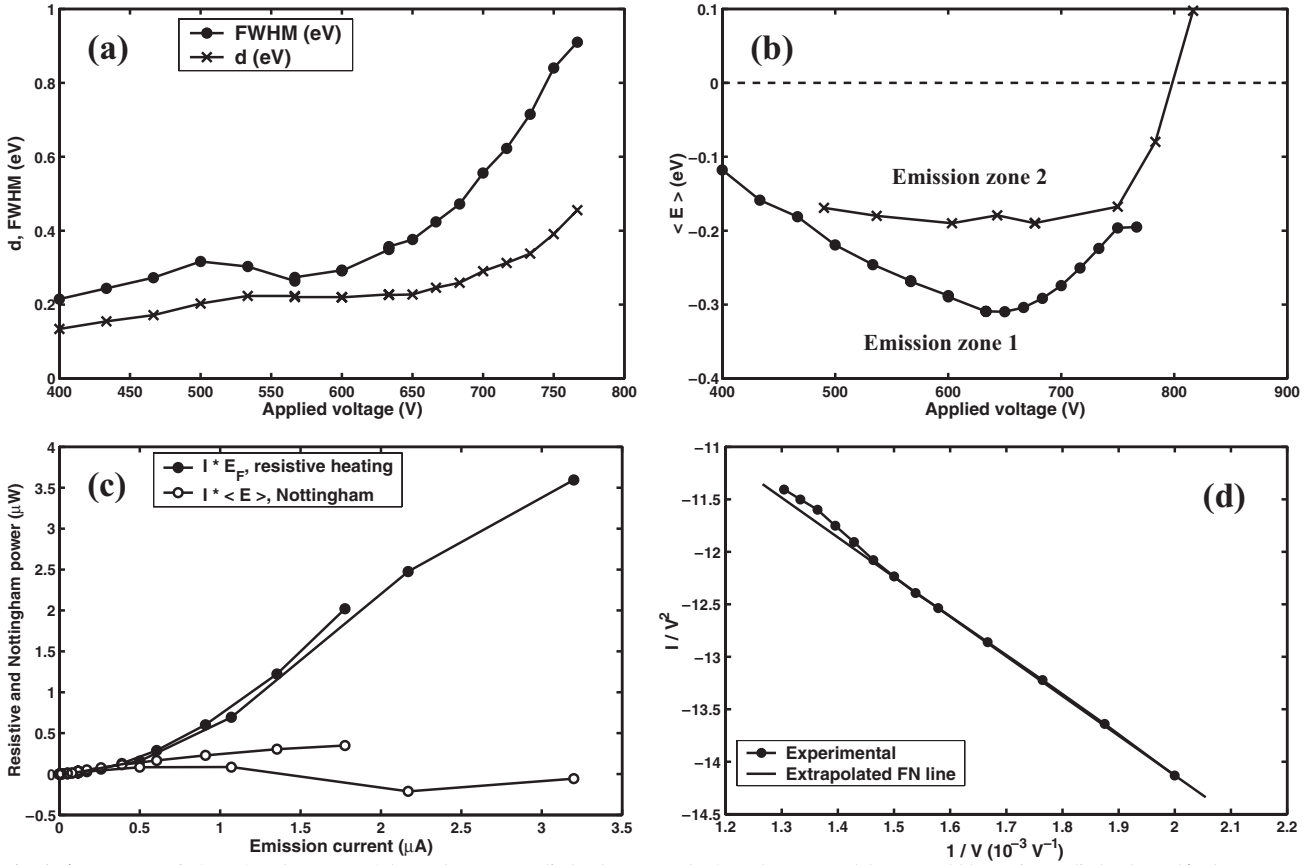

Fig. 6. a) Parameter d of Eq. 1 and FWHM of the peak versus applied voltage. For the free electron model one would have d α applied voltage. b) The average energy with respect to the local Fermi energy for TEDs from two different zones versus applied voltage. c) The Nottingham and resistive powers calculated with $I_{FE}<E>$ and $I_{FE}E_F$ (see text). d) FN plot corresponding to Fig. 5a. The current rises above the FN line because of the current-induced high temperature.

low similarly shaped curves, and are not linear in applied voltage as expected by the simple theory. The values here are larger than previously measured,[30,51] reaching 0.8 eV because of the inclusion of measurements going to higher field and temperature that widen the spectra further. The FWHM is of technical importance because it is an important parameter for point electron sources and in particular chromatic aberration. The widening means there will be a tradeoff in the use of CNTs at high current as high brightness point sources. The nonlinearity of d will be discussed below in relation to the work function.

Another way to analyze this data is to integrate the TEDs to find the average energy $\langle E \rangle$ of the emitted electrons with respect to the local E_F at the cap determined from the TED fits. This is useful for estimating the Nottingham effect.[32] $\langle E \rangle$ versus applied voltage is plotted in Figure 6b for the TEDs of Figure 5a, and another series for zone 2. A positive $\langle E \rangle$ means cooling and a negative $\langle E \rangle$ means heating. The two zones have significant differences. As the voltage increases, $\langle E \rangle$ first decreases as the field widens the TEDs on the low energy side, and then it increases as the nanotube heats causing the TEDs to widen on the high energy side. This reduces Nottingham heating. In Figure 6c is shown the dissipated Nottingham power if all electrons were emitted with these TEDs ($P_N \equiv I_{FE}\langle E \rangle$) and the resistive power $P_R \equiv I_{FE}{}^2R = I_{FE}E_F$. However, one must carry out laborious measurements of the spectra and local current over the whole cap to determine the total Nottingham heat balance. As discussed below, these curves overestimate Nottingham heating. However, it is clear that the resistive heating is less than Nottingham heating at low current but dominates in the high temperature range.

One of the consequences of the heating is that the current rises above the FN line at high voltages.[47] A FN plot is shown in Figure 6d. At lower voltages, it follows well the linear FN equation of $\ln(I/V^2) \propto -1/V$. However, at the higher voltages, I_{FE} first increases significantly above the FN line at $T_A \approx 1000$ K. This is the direct consequence of the well known increase of $I_{FE} \propto T^2$ in FN theory.[31] In Figure 7a the difference between the FN fit at low voltage and the measured data is plotted against the measured T_A. The fit to the T^2 law is rather good except for the last two points. These points mark the temperature at which the MWNT undergoes changes, in particular length reduction by partial destruction (see below).

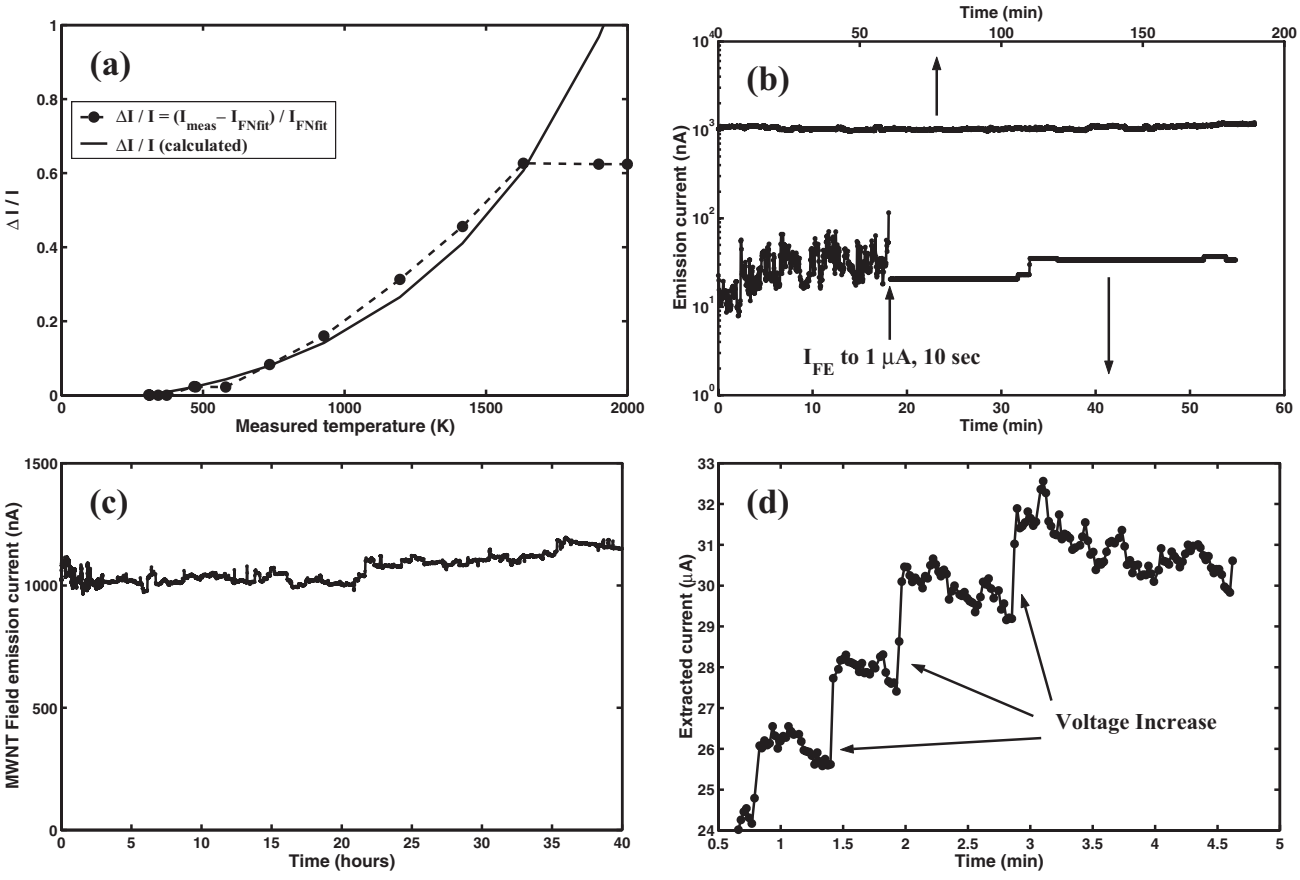

Fig. 7. a) Difference between the measured current and the low current fit to the FN plot as a function of T_A. The difference follows closely the expected T^2 law for FN tunneling until the last two points where the very high temperatures degrade the MWNT. b) Current stability measured before and after a current-induced heat flash of 10 s and a 3 h current stability run at 1 μA. c) Current stability measured for 40 h in UHV. Linear y-axis. d) Current versus time when the several nanotubes are shortening due to high temperatures induced by the emission current. Each rise is due to an increase by 10 V in the extraction voltage.

A second consequence of the heating is an increase in FE current stability. In Figure 7b it is shown that the I_{FE} induced heating can be used to thermally remove adsorbates allowed to accumulate by exposure to a poor vacuum. To demonstrate this, the pumping was stopped for twenty minutes allowing the vacuum to degrade to about 10^{-7} Torr. This led to the extremely unstable current at the bottom of Figure 7b. After a 10 s flash at 1 μA FE current, which according to the TEDs raised the temperature to ~1000 K, the current became as stable as before. I_{FE} is even more stable at higher current because the hot nanotube prevents re-adsorption as is well known for Schottky emitters. Figure 7b and c shows an almost perfect stability obtained at 1 μA over three hours and excellent stability over 40 h. The treatment at 1 μA thus has an effect comparable with a flash surface cleaning, but without any external heat source.

The destruction of the CNTs noted above has considerable importance for using nanotubes in applications because it fixes their current limits. While it is seen that the self-heating made it possible to obtain a very good current stability, it became unstable at even higher currents and thus higher temperatures. Recently, several groups have used electron microscopy to directly observe the destruction of nanotubes for very strong emission currents. In the period before we had identified and quantified Joule heating to high temperatures, Wei et al.[52] made observations in a scanning electron microscope (SEM) on MWNTs produced by CVD during FE, and observed a reduction in length of the nanotube for currents between 200 nA and 1 μA. Also Wang et al.[53] made observations of arc electric MWNTs inside a transmission electron microscope (TEM) permitting higher resolution. They observed destruction for even higher currents of about 200 μA (also much higher than ours). Their better resolution made it possible to see abrupt length reductions, sharpening, splitting of the MWNT, and also tearing of an external layer of graphite in certain cases. Similar to Dean et al.[47] we also observed the progressive destruction of the nanotubes by the reductions in emission current at constant voltage. Figure 7d shows the high current trend versus time as the voltage is raised by 10 V steps approximately every 30 s. At each voltage increase the current first jumps up and then decays in a noisy way. This is attributed to length reduction as in the microscopy studies, and the cause can now be identified as high-temperature breaking or evaporation at the nanotube end. The higher currents obtained by Wang et al. are then because their arc electric nanotubes had much lower electrical resistance. As reported previously,[33] these high temperatures cause the emission of light visible by eye in a darkened room. The observed light emission came precisely from a point at the end of the Ni base tip starting at I_{FE} ~ 1.2 μA (T_A ~ 1500 K). It increased in intensity as I_{FE} was raised. Light emission from MWNTs during FE has been previously observed.[1,54] Both incandescence[1] due to resistive heating (but without experimental proof) and fluorescence from apex resonant states have been proposed.[54] Because of the association with high T_A and a modelization based on the measured resistance and current, the light emission here is clearly an incandescence effect. Note that no resonance-like tunneling states were detectable in the TEDs after the high temperature cleaning. Originally, only one point of light was seen for currents in the μA range,[33] but as the emissions from the highest field nanotubes were reduced by high temperature induced shortening, even more nanotubes could be made to emit light simultaneously. Figure 8b shows light emission from several MWNTs on the Ni tip. Also shown is that the light emission can be shifted between different MWNTs by shifting the voltage balance between the split extraction anodes to promote emission from MWNTs on different sides on the Ni tip.

Planck's law was used to calculate that, at the observation distance of 20 cm, ca. 10^5 photons per second should be seen, well within the sensitivity of the human eye. Re-

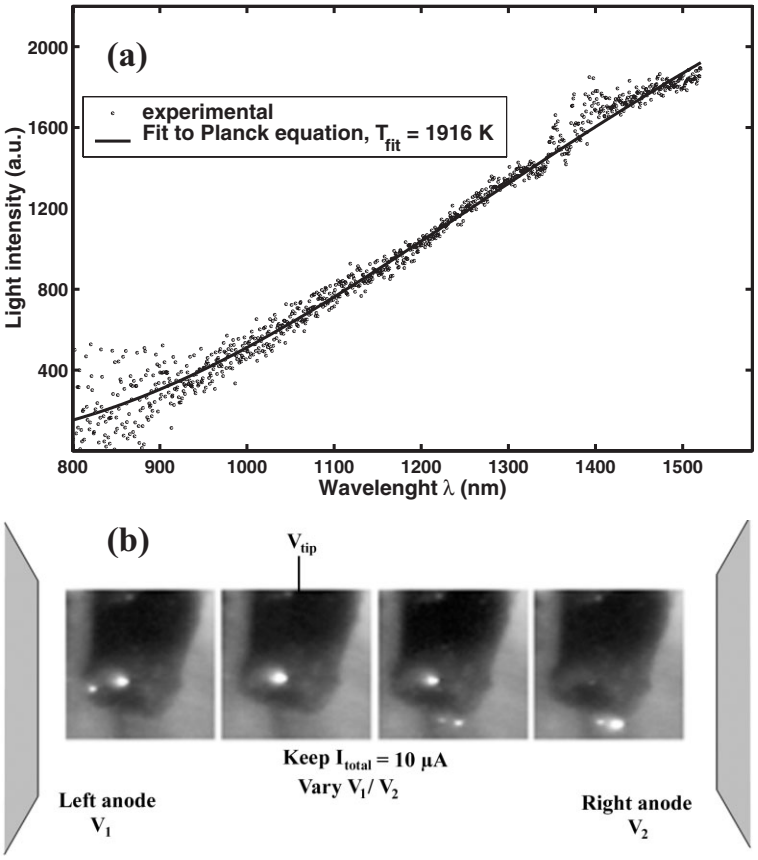

Fig. 8. a) Optical spectra of a few MWNTs heated by field emission at 10 μA. b) Changing the balance between various hot MWNTs as the field strength is shifted from left to right. I_{FE} = 10 μA.

cent optical spectroscopy measurements of light emission from a MWNT layer from which a small number of emitters were active confirmed that the light has a black-body spectrum.[55] The authors were able to estimate temperature in the range 1500–2000 K, depending on the emitted current. Figure 8a shows an optical spectra measured from a few CNTs in a different vacuum system on the same MWNT covered Ni tip for 10 μA total current. The fit to the Planck law gives a temperature in the range expected from the TED fits at this current. Such a good agreement is at first surprising for a multi-CNT emission but this occurs since if other emitters are active at significantly lower temperatures they emit much less light because of the T^4 radiation law, and emitters cannot reach higher temperatures because that causes nanotube shortening.

The light was also observed during the programmed destruction of a single nanotube to measure its maximum supportable current. In this case the total current was raised in steps of 10 s until it reached 110 μA during simultaneous optical observation. Four to six bright MWNTs were visible. The brightest light emitter then started to increase in intensity by itself on a time scale of a few seconds, until it suddenly disappeared at the same time that the total current dropped by 40 μA. This sudden breakdown differs from the gradual shortening that we discussed above, and shows that CNTs may behave differently depending on which parameter set of current and time is used. The measure of 40 μA defines a current maximum for this one MWNT. However, a current maximum must be defined with some care because, as shown above, if the current steps are too slow the nanotube reduces gradually in length when it reaches a high temperature.

3. Discussion

3.1. Field Emission from Nanostructures on MWNT Caps

As stated above, FE from nanostructures can be qualitatively understood by referring to a simple energy diagram for resonant tunneling often drawn in the literature.[38,56] The emission is considered to occur through local bound states that exist within the nanostructure,[31] and which shift because of field penetration.[57] The weakness of this analysis is that the chemical composition and structure of the nanostructure is not known, and no electronic structure calculations have been carried out to confirm the validity of such a simple picture, as has been done for adsorbed atoms on clean metal surfaces.[31] That said, within the simple picture one understands the resulting FN plots which can be highly bowed and curve up as each new resonant state arrives at the Fermi level by field shifting.[56] The supply function then switches from empty to filled states. The idea of FE through resonant tunneling states on the CNTs has already been suggested.[20,25,26] What is emphasized here is that these effects continue to exist even when the MWNTs are heated to quite high temperatures, and after field evaporation has removed an appreciable length of the MWNT. This leads us to propose that for these treatments the nanostructures are themselves composed of disordered carbon atoms. In the first case, the heat treatment is not sufficient to allow the carbon atoms to restructure because of their very high activation energies for atomic movement. In the second case, the field desorption of covalent materials is known to pull off whole clusters of atoms and leave a relatively disordered surface.[58] In both cases the covalent nature of the carbon increases the tendency to form nonconducting nanostructures and resonant tunneling states. These structures can develop voltage drops of the order of volts, even under the very ideal conditions of ultrahigh vacuum (UHV) and high temperature. The difficulty in removing them even under UHV conditions may be connected to the great amount of attention the nanotube community has paid to establishing low contact resistances to CNTs.[59]

3.2. Estimations of $\rho(T)$ and $\kappa(T)$

One of the most exciting possibilities of the TED measurements of temperature and resistance is that it should allow a simultaneous estimation of the temperature dependence of both the resistivity, $\rho(T)$, and the thermal conductivity, $\kappa(T)$, a unique advantage for FE. Our original simulations were made with the spirit of showing that resistive heating, radiation, and thermal conduction could explain the main features of the measurements.[34] To do this the temperature profiles along the nanotube were simulated for different currents to fit the experimental $T_A(I_{FE})$ and $R(T_A)$ curves by iteratively varying the functions $\rho(T)$ and $\kappa(T)$. In the original fits, however, $\kappa = 100$ W K^{-1}·m^{-1} was taken from the literature and fixed, whilst a linear dependence for the resistance, $R=R_0-\alpha T$, was used. The fits could have been much better, especially for $R(T)$. In Figure 5c and d it is shown that much better fits to both data sets can be obtained if better functions for $\rho(T)$ and $\kappa(T)$ are used. $\rho(T)$ is now an exponentially decreasing function, and $\kappa(T)$ linearly increases with T (see Fig. 9a). The average values are both in the range of disordered graphite,[60] which can be understood from the TEM images showing many defects. $\kappa(T)$ is roughly ten times lower than that used in the original simulations. The length and diameter of the MWNT are rather approximate so the absolute values are crude. However the ratios and general temperature dependence do not vary strongly with the nanotube dimensions and thus these simulations provide a proof-of-concept for the technique.

At first glance the function for $\kappa(T)$ appears not to have a physical basis. For high-quality crystals $\kappa(T)$ peaks typically at ca. 1/20 of the Debye temperature θ_D,[61] and falls at higher temperature. However, this peak diminishes and displaces to higher temperature when mean free paths are reduced due to finite CNT length or defects.[62] For very

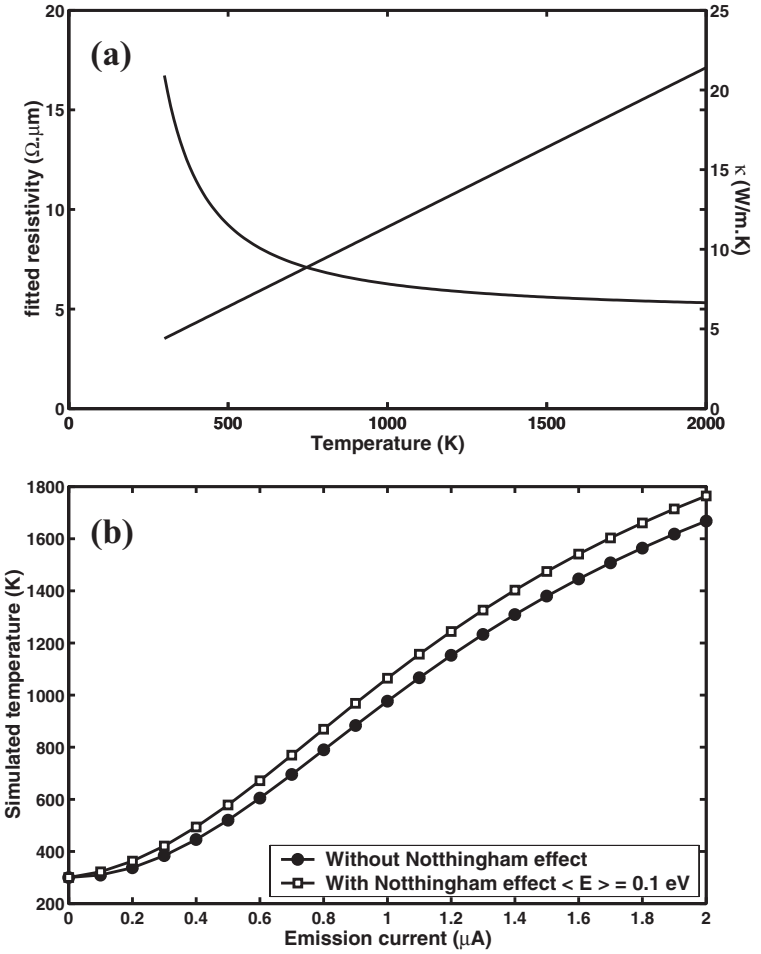

Fig. 9. a) $\rho(T)$ and $\kappa(T)$ used for the simulations that fitted the plots of $T_A(I_{FE})$ in Fig. 5c) and $R(T_A)$ in Fig. 5d). b) Simulations of the heat problem with and without Nottingham heating (see text).

short phonon mean-free paths the peak disappears completely, and $\kappa(T)$ should then resemble the classic curve for specific heat. It is interesting to note that carbon is special in that the specific heat does not sharply saturate at θ_D but continues to rise even up to 3000 K.[60] More datasets with a better knowledge of the length and radius are needed to confirm and expand this result, and probably the inclusion of other terms in the heat problem such as the Nottingham effect.

3.3. Nottingham Effects

One cannot immediately neglect Nottingham effects in the heat problem on the basis of the measurements in Figure 6c and d, which show it is appreciably less than resistive heating over a wide current range. This is because it occurs at the MWNT cap where it would have a maximum effect on the temperature measured by the TEDs. Originally, some preliminary simulations were carried out that included the Nottingham effect, using the assumption that $P_N = I_{FE}\langle E\rangle$ with $\langle E\rangle$ fixed at –0.1 eV.[34] Mathematically it was included as a boundary condition at the free end. Corrections to the calculated temperatures of less than 10 % at 2000 K were found (see Fig. 9b). This is appreciable but still of second order. However, at low temperature and for small nanotubes the Nottingham effect could dominate over both resistive and radiation effects. In contrast, Svenningsson et al.[63] have recently published calculations of the Nottingham effect over a wider temperature range based on the similar assumptions for P_N, except that $\langle E\rangle$ was theoretically calculated based on estimates of the β factor from their FN plot. They also fixed $\kappa(T)$ and based their $\rho(T)$ on our measured values for $R(T_A)$. They found Nottingham cooling to be much more important, being even more important than radiation cooling for their chosen nanotube parameters. This discrepancy may be due to the different nanotube dimensions because this can change the predominance between different mechanisms. This highlights the need for more calculations based on knowledge of all the parameters of the CNT.

The problem with using $P_N = I_{FE}\langle E\rangle$ for the whole current at the center of the tip is that it overestimates the heating, because away from the center of the emission the field is lower, which narrows the TEDs on the low-energy side and hence decreases heating (and hence lowers $\langle E\rangle$ on the low-energy side). If $\langle E\rangle > 0$, cooling occurs. Complex calculations and measurements of the current, field, temperature, and energy distributions over the cap and along the near shank, taking into account the parameters of the nanotube (length, radius, resistance, cap geometry), must be carried out to correctly quantify this effect. This is especially delicate because, as is seen in Figure 6b and c, the Nottingham effect can switch from cooling to heating over a small current range.

3.4. Stability in the Presence of Induced Heating

The stable, high value of T_A found raises an interesting point for FE in general. This is the only example in FE literature that can be found of observations of FE-induced stable heating of the emitter body to any temperature above ambient, let alone to 2000 K. We propose that this is because of two parameters of MWNTs that differ from those of metal emitters, and which lead to I_{FE} runaway and thus emitter breakdown. Firstly, the resistance of metals increases roughly linearly with temperature, which means a positive heating feedback once I_{FE}-induced heating starts. Secondly, a combination of high temperature and field

usually induces the well-known mechanism of field-driven sharpening of tips by surface diffusion, which in turn increases the field and hence creates positive feedback for I_{FE}. This creates an extremely unstable situation, and metal FE tips generally breakdown at high I_{FE} without warning. In contrast, the resistance of this MWNT was shown to be decreased substantially with temperature, which gives a negative feedback to heating, and secondly surface diffusion is much slower for covalent carbon which inhibits the field-driven sharpening.

3.5. Nanotube Destruction

Dean et al.[47] have proposed that length reduction is due to thermally-assisted field evaporation instead of normal evaporation. This would help to explain why the nanotubes degrade at temperatures much lower than those needed for normal evaporation of carbon, and why it occurs principally at the nanotube end where the field is the highest. Simple evaporation may still be an important mechanism because carbon atoms at a disordered cap or at defect sites will have fewer nearest neighbors, and thus have lower sublimation energies than carbon on a graphite surface. The images of Wang et al.[53] show that the destruction of the nanotube can proceed by the abrupt changes in, and the breaking off of, small sections. This can occur after weakening further down the shank at defect sites where the field is too low to invoke field evaporation. Note also that local resistive heating would be enhanced at such sites. In such a case the force of the field may assist the degradation by tearing off larger pieces of the nanotube, without being a field evaporation at an atomic level. The nanotube shortening is gradual when compared to the breakdown of a metal tip but it is not a removal atom by atom.

We argued that resistive heating and not local heating by Nottingham effects is the important mechanism in the creation of current-induced, stable, high temperatures. However one can speculate that Nottingham effects may be important in a different context, that is during the destruction process itself. During the destruction, the current is very unstable (Fig. 7d) and does not undergo a gradual decrease, as with a slow evaporation process. Again, from the images of Wang et al., this could simply be due to sudden increases or decreases in the amplification factor, β, as the nanotube splits or shortens. However, as shown above, field evaporation causes the creation of nanostructures, resonant tunneling, and local heating at low currents. If such nanostructures are also formed during the destruction process as a consequence of the MWNT breaking, then very strong local heating effects would be created almost instantaneously, and thus appreciably increase the instability and temperature of the cap region. A predominance of local Nottingham effects in MWNT destruction, as opposed to a field evaporation, can explain why no nanotube shortening was seen when electron bombardment was used repeatedly at up to 1600 K, even though the voltage applied to attract electrons to the tip creates a positive field on the MWNT three to four times higher than that used during electron emission. In a positive field there are no local emission Nottingham effects. TED measurements during the destruction process would be useful in studying this idea.

3.6. Work Function

There are numerous published values for the work function, ϕ, of different types of CNTs. Actually, ϕ is a local parameter and it is not clear that it can be well defined for many CNT caps that have very rough structures on the nanometer scale. In addition, there is the problem of patch fields.[64] That said, several authors have combined the $I(V)$ curves and the TED data to give both ϕ and the amplification factor, β.[20,51] (Other authors simply estimated β from an approximate knowledge of the emitter geometry, which is somewhat hazardous). In principle, the slope of the FN plot gives $m \approx 0.5 \times \phi^{3/2}/\beta$ and the TEDs give $d \approx F_0/\sqrt{\phi}$. However, there are serious problems with this method even for clean metal emitters.[31,32] The first is that the deviation from free electron behavior particularly affects the value of d in Equation 1. This is very pronounced for carbon, as can be seen from the measured TEDs here which have very large shoulders on the low energy sides. The plot for d in Figure 6a shows that d is not even linear in $F = \beta V$. Depending on which value of d is chosen, values of ϕ from 3.8 to 4.7 eV for lower voltages, and up to 6.8 eV at high voltage, were found. There is obviously an even greater problem when nanostructure TEDs are used to estimate d, as shown in the literature.[20] In principle, β can be measured independently by the "best image voltage" in FIM.[65] Such a measurement was carried out with Ar as an imaging gas, and from the FN plot it was found that $\phi = 6.1$ eV. We proposed that this value is also false because of the second problem, which is that the FN equation must be corrected when the emitting radius is in the range of the width of the tunneling barrier.[66] This effect gives a higher slope to the FN plot and hence causes an overestimation of ϕ.

Two recent articles propose completely different methods for measuring ϕ. Suzuki et al.[67] used electron microscopy to excite photoemission, while Zhi et al.[68] used an elegant method to measure ϕ that exploited mechanical vibrations to measure the contact potential difference between various carbon nanotubes and gold contacts. However, it seems logic that these methods measure the average ϕ over the whole nanotube and not at the emission zone, which is what counts for field emission. Also, it is not clear that surface adsorbates were fully removed, which is a prerequisite for work function measurements. To summarize, we argue that there is still no viable measure for the CNT FE work function, and it is still best to use $\phi = 4.9$ eV for graphite.

3.7. Modeling the Radiation Losses

The radiation losses have been modeled[34,50,63] by a differential surface area and the Stefan-Boltzmann law. This is clearly wrong for nanotubes whose lateral dimensions are shorter than the wavelength of the emitted light or the photon mean free path. This means there is a need to consider photon emission within the framework of Rayleigh scattering theory[69] where for small particles the absorption is proportional to the volume. This may completely change the balance between radiation, thermal conduction, and Nottingham effects.

4. Conclusions

In this article we have tried to bring out the advances in our understanding of field emission from nanotubes, and point out where more work is needed. The nanostructures that lead to resonant tunneling-like effects are very common and robust on MWNTs. As well as degrading current stability in FE devices above the nA range, they are also one of the principal impediments to using FEES to measure the intrinsic properties of nanotubes and nanowires. The problem is that the high temperature and field treatments often also remove the nanotubes or nanowires that have been attached to base tips by gluing or van der Waals forces (though they did not remove the MWNTs grown directly on massive Ni tips). It is important then to develop a methodology permitting a consistent and benign cap-cleaning process.

For the cleaned emitters, in retrospection, what distinguishes CNTs is not dramatic effects in the $I(V)$s or TEDs due to the their novel electronic structure, but their ability to function over long times under a condition of current-induced high temperature.[33,47] It has been argued before that the intrinsic decrease in the MWNT resistance with temperature and low surface diffusion of carbon prevents them from falling immediately into a current runaway and explosive breakdown common to metal emitters.[70–72] The nanotube resistive heating is a tool to preferentially clean the principal emitters in an ensemble without external heating. This may be the reason that such excellent stability has been achieved in CNT flat screens where the vacuum conditions are far from UHV. The gradual length reduction at higher currents provides a tool for more uniform emission from a multi-nanotube emitter at the price of higher extraction voltage. This is useful in applications such as displays where uniformity is critical.

Modelization of the heat transport problem is essential for exploiting the FEES data to extract simultaneous estimates of the physical parameters of CNTs. It has permitted estimates of $\rho(T)$ and $\kappa(T)$ together for the first time. Measurements on different types of CNTs with a better characterization of their crystalline structure and dimensions are now needed so that more quantitative calculations can be made. The theory can then be extended to better include advanced models of the Nottingham effects and radiation cooling.

In conclusion, the combination of $\rho(T)$ and $\kappa(T)$ estimates, the optical emissions, and the in situ excitation of mechanical resonances[43] now gives FE access to four fundamental characteristics of a single nanotube or nanowire. These methods are currently being applied to SWNTs and high-quality semiconducting nanowires.

5. Experimental

Oriented MWNTs were grown by CVD directly on large Ni tips that had been previously electrochemically etched in an HCl solution. The Ni tip was covered by MWNTs, but oriented growth was achieved at the Ni tip apex by flowing the gas along the tip axis during the CVD. The CVD consisted of the decomposition of acetylene mixed with 80 % N_2 at 870 K. By this method the MWNTs were securely mechanically and electrically bound to the substrate. SEM images showed that the apex MWNTs were quite straight, with diameters in the range 20–50 nm and lengths of up to 40 μm. The multiwalled character, diameter range, and high number of defects of the MWNTs was confirmed using a TEM with samples fabricated by exactly the same procedure.

The FE experiments were carried out in a UHV system with a base pressure of ca. 7×10^{-11} Torr. The Ni tip was held in a W spiral to allow in-situ cleaning by standard Joule heating to ca. 1300 K. A circular cathode loop placed in front of the tip was used to heat the tip at up to 1600 K by electron bombardment. Field desorption was also used to try to clean the nanotubes. FEM and FIM patterns were observed on a multichannel plate (mcp) placed 35 mm from the tip. I_{FE} was measured by: 1) the total current leaving the tip; 2) letting the emission strike a polarized metal plate connected to a picoampere meter; and 3) integrating the TEDs. The TEDs were measured with an hemispherical electron energy analyzer through a probe hole in the same UHV system. Mechanical displacements of the FE head allowed us to change quickly in-situ between imaging with the mcp or probe hole measurements with the energy analyzer. The combination of mechanical and electrostatic deflection with the quadrapole extraction anode allowed a precise centering and alignment of different parts of the emission pattern to the probe hole. The temperature of the Ni base tip versus the current in the heating spiral or during the electron bombardment was determined by optical micropyrometry in the range 920–1600 K.

Though many MWNTs are present on the Ni tip, the FE experiments are specific to an individual one. This is firstly because I_{FE} is a strongly exponential function of field and hence only a few MWNTs that protrude furthest to the anode or which have a sharper apex radius will emit. Secondly, the radial projection geometry of FE means that even if several MWNTs emit they are in general projected at different angles and can be distinguished with ease in the FE pattern and at the probe hole which subtends an angle of only 4°. In fact, for most of our studies there was only one MWNT emitting. After it was shortened by field desorption, another one appeared at the resulting higher voltages, which emitted at a different angle. It contributed between 10 and 25 % of the total current, depending on the voltage range. The separation of currents emitted from the two different MWNTs was estimated by letting only specific parts of the pattern strike the measuring plate or the mcp.

The general experimental procedure was as follows: 1) tip treatment; 2) FEM and perhaps FIM observations; 3) $I(V)$ and $I(t)$ measurements; 4) FEES measurements after positioning the desired part of the FEM pattern on the probe hole; and 5) new tip treatment and repetition of the measurement cycle.

Received: November 9, 2005
Final version: February 24, 2006

[1] A. G. Rinzler, J. H. Hahner, P. Nikolaev, L. Lou, S. G. Kim, D. Tomanek, P. Nordlander, D. T. Colbert, R. E. Smalley, *Science* **1995**, *269*, 1550.
[2] W. de Heer, A. Châtelain, D. Ugarte, *Science* **1995**, *270*, 1179.
[3] L. A. Chernozatonskii, Y. V. Gulyaev, Z. J. Kosakovskaja, N. I. Sinitsyn, G. V. Torgashov, Y. F. Zakharchenko, E. A. Fedorov, V. P. Val'chuk, *Chem. Phys. Lett.* **1995**, *233*, 63.

[4] W. B. Choi, D. S. Chung, J. H. Kang, H. Y. Kim, Y. W. Jin, I. T. Han, Y. H. Lee, J. E. Jung, N. S. Lee, G. S. Park, J. M. Kimd, *Appl. Phys. Lett.* **1999**, *75*, 3129.
[5] K. A. Dean, B. F. Coll, Y. Wei, C. G. Xie, A. A. Talin, J. Trujillo, J. E. Jaskie, *Proc. 21st Int. Display Res. Conf.* **2001**, 1225.
[6] D.-S. Chung, S. H. Park, H. W. Lee, J. H. Choi, S. N. Cha, J. W. Kim, J. E. Jang, K. W. Min, S. H. Cho, M. J. Yoon, J. S. Lee, C. K. Lee, J. H. Yoo, J.-M. Kimb, J. E. Jung, Y. W. Jin, Y. J. Park, J. B. You, *Appl. Phys. Lett.* **2002**, *80*, 4045.
[7] J. Dijon, C. Bridoux, A. Fournier, F. Geffraye, T. Goislard de Monsabert, B. Montmayeul, M. Levis, D. Sarrasin, R. Meyer, K. A. Dean, B. F. Coll, S. Johnson, C. Hagen, J. Jaskie, *J. Soc. Inf. Display* **2004**, *12*, 373.
[8] Y. Saito, S. Uemura, K. Hamaguchi, *Jpn. J. Appl. Phys., Part 2* **1998**, *37*, L346.
[9] M. Croci, I. Arfaoui, T. Stockli, A. Chatelain, J.-M. Bonard, *Microelectron. J.* **2004**, *35*, 329.
[10] N. de Jonge, Y. Lamy, K. Schoots, T. H. Oosterkamp, *Nature* **2002**, *420*, 393.
[11] K. Hata, A. Takakura, Y. Saito, *Surf. Interf. Anal.* **2004**, *36*, 506.
[12] G. Pirio, P. Legagneux, D. Pribat, K. B. K. Teo, M. Chhowalla, G. A. J. Amaratunga, W. I. Milne, *Nanotechnology* **2002**, *13*, 1.
[13] M. A. Guillorn, M. D. Hale, V. I. Merkulov, M. L. Simpson, G. Y. Eres, H. Cui, A. A. Puretzky, D. B. Geohegan, *Appl. Phys. Lett.* **2002**, *81*, 2860.
[14] K. B. K. Teo, L. Hudanski, F. Peauger, J.-P. Schnell, L. Gangloff, P. Legagneux, D. Dieumegard, G. A. J. Amaratunga, W. I. Milne, *Nature* **2005**, *437*, 968.
[15] G. Z. Yue, Q. Qiu, B. Gao, Y. Cheng, J. Zhang, H. Shimoda, S. Chang, J. P. Lu, O. Zhou, *Appl. Phys. Lett.* **2002**, *81*, 355.
[16] R. Rosen, W. Simendinger, C. Debbault, H. Shimoda, L. Fleming, B. Stoner, O. Zhou, *Appl. Phys. Lett.* **2002**, *76*, 1668.
[17] C. Dong, G. R. Myneni, *Appl. Phys. Lett.* **2004**, *84*, 5443.
[18] E. Minoux, O. Groening, K. B. K. Teo, S. H. Dalal, L. Gangloff, J.-P. Schnell, L. Hudanski, I. Y. Y. Bu, P. Vincent, P. Legagneux, G. A. J. Amaratunga, W. I. Milne, *Nano Lett.* **2005**, *5*, 2135.
[19] D. Lovall, M. Buss, E. Graugnard, R. P. Andres, R. Reifenberger, *Phys. Rev. B* **2000**, *61*, 5683.
[20] M. J. Fransen, T. L. van Rooy, P. Kruit, *Appl. Surf. Sci.* **1999**, *146*, 312.
[21] J.-M. Bonard, H. Kind, T. Stöckli, L.-O. Nilsson, *Solid State Electron.* **2001**, *45*, 893.
[22] N. de Jonge, J.-M. Bonard, *Phil. Trans. R. Soc. Lond. A* **2004**, *362*, 2239.
[23] J.-M. Bonard, K. A. Dean, B. F. Coll, C. Klinke, *Phys. Rev. Lett.* **2004**, *89*, 197 602.
[24] K. A. Dean, B. R. Chalamala, *Appl. Phys. Lett.* **2000**, *76*, 375.
[25] K. A. Dean, P. von Allmen, B. R. Chalamala, *J. Vac. Sci. Technol. B* **1999**, *17*, 1959.
[26] J.-M. Bonard, J. P. Salvetat, T. Stöckli, L. Forro, A. Chatelain, *Appl. Phys. A* **1999**, *69*, 1.
[27] Y. Saito, K. Hata, T. Murata, *Jpn. J. Appl. Phys., Part 2* **2000**, *39*, L271.
[28] K. A. Dean, O. Groening, O. M. Kittel, L. Schlapbach, *Appl. Phys. Lett.* **1999**, *75*, 2773.
[29] C. Oshima, K. Matsuda, T. Kona, Y. Mogama, M. Komaki, Y. Murata, T. Yamashita, Y. Saito, K. Hata, A. Takakura, *Jpn. J. Appl. Phys., Part 2* **2001**, *40*, L1257.
[30] A. Takakura, K. Hata, Y. Saito, K. Matsuda, T. Kona, C. Oshima, *Ultramicroscopy* **2004**, *95*, 139.
[31] J. W. Gadzuk, E. W. Plummer, *Rev. Mod. Phys.* **1973**, *45*, 487.
[32] L. W. Swanson, A. E. Bell, in *Advances in Electronics, Electron Physics*, Vol. 32 (Ed: L. Marton), Academic Press, New York **1973**, 193.
[33] S. T. Purcell, P. Vincent, C. Journet, V. T. Binh, *Phys. Rev. Lett.* **2002**, *88*, 105 502.
[34] P. Vincent, S. T. Purcell, C. Journet, V. T. Binh, *Phys. Rev. B* **2002**, *66*, 075 406.
[35] E. Muller, *Sci. Am.* **1952**, *186*, 58.
[36] J. A. Becker, *Adv. Catal.* **1955**, *7*, 136.
[37] S. K. Sekatskii, V. S. Letokhov, *J. Expt. Theor. Phys.* **2002**, *95*, 210.
[38] L. W. Swanson, L. C. Crouser, *Surf. Sci.* **1970**, *23*, 1.
[39] C. B. Duke, M. E. Alferieff, *J. Chem. Phys.* **1967**, *46*, 923.
[40] S. T. Purcell, V. T. Binh, R. Baptist, *J. Vac. Sci. Technol. B* **1997**, *15*, 1666.
[41] K. Nagaoka, H. Fujii, K. Matsuda, M. Komaki, Y. Murata, C. Oshima, T. Sakurai, *Appl. Surf. Sci.* **2001**, *182*, 5.
[42] Y. Saito, R. Mizushima, K. Hata, *Surf. Sci.* **2002**, *499*, L119.
[43] S. T. Purcell, P. Vincent, C. Journet, V. T. Binh, *Phys. Rev. Lett.* **2002**, *89*, 276 103.
[44] S. T. Purcell, V. T. Binh, N. Garcia, *Appl. Phys. Lett.* **1995**, *67*, 436.
[45] W. P. Dyke, W. W. Dolan, in *Advances in Electronics, Electron Physics*, Vol. 8 (Ed: L. Marton), Academic Press, New York, **1956**, p. 89.
[46] S. T. Purcell, unpublished.
[47] K. A. Dean, T. P. Burgin, B. R. Chalamala, *Appl. Phys. Lett.* **2001**, *79*, 1873.
[48] C. Oshima, K. Matsuda, T. Kona, Y. Mogama, M. Komaki, Y. Murata, T. Yamashita, T. Kuzumaki, Y. Horiike, *Phys. Rev. Lett.* **2002**, *88*, 038 301.
[49] R. D. Young, *Phys. Rev.* **1959**, *113*, 110.
[50] N. Y. Huang, J. C. She, J. Chen, S. Z. Deng, N. S. Xu, H. Bishop, S. E. Huq, L. Wang, D. Y. Zhong, E. G. Wang, D. M. Chen, *Phys. Rev. Lett.* **2004**, *93*, 075 501.
[51] N. de Jonge, M. Allioux, M. Doytcheva, M. Kaiser, K. B. K. Teo, R. G. Lacerda, W. I. Milne, *Appl. Phys. Lett.* **2004**, *85*, 1607.
[52] Y. Wei, C. Xie, K. A. Dean, B. F. Coll, *Appl. Phys. Lett.* **2001**, *79*, 4527.
[53] Z. L. Wang, P. Poncharal, W. A. de Heer, *Microsc. Microanal.* **2000**, *6*, 224.
[54] J.-M. Bonard, T. Stöckli, F. Maier, W. A. de Heer, A. Châtelain, J.-P. Salvetat, L. Forró, *Phys. Rev. Lett.* **1998**, *81*, 1441.
[55] M. Sveningsson, M. Jonsson, O. A. Nerushev, F. Rohmund, E. E. B. Campbell, *Appl. Phys. Lett.* **2002**, *81*, 1095.
[56] S. T. Purcell, V. T. Binh, N. Garcia, M. E. Lin, R. P. Andres, R. Reifenberger, *Phys. Rev. B* **1994**, *49*, 17259.
[57] A. J. Bennett, L. M. Falicov, *Phys. Rev.* **1966**, *151*, 512.
[58] M. K. Miller, A. Cerezo, M. G. Hetherington, G. D. W. Smith, *Atom Probe Field Ion Microscopy*, Oxford University Press, Oxford, UK **1996**.
[59] Y. Zhang, N. Franklin, R. Chen, H. Dai, *Chem. Phys. Lett.* **2000**, *331*, 35.
[60] B. T. Kelly, *Physics of Graphite*, Applied Science, London **1981**.
[61] C. Kittel, *Introduction to Solid State Physics*, 3rd ed., John Wiley & Sons, New York **1968**.
[62] P. Chantrenne, J. L. Barrat, X. Blase, J. D. Gale, *J. Appl. Phys.* **2005**, *97*, 104 318.
[63] M. Sveningsson, K. Hansen, K. Svensson, E. Olsson, M. Jonsson, E. E. B. Campbell, *Phys. Rev. B.* **2005**, *72*, 085 429.
[64] R. D. Young, H. E. Clark, *Phys. Rev. Lett.* **1966**, *17*, 351.
[65] E. W. Muller, T. T. Tsong, *Field Ion Microscopy*, American Elsevier, New York **1969**.
[66] C. J. Edgecombe, *Ultramicroscopy* **2003**, *95*, 49.
[67] S. Suzuki, Y. Watanabe, Y. Homma, S. Fukuba, S. Heun, A. Locatelli, *Appl. Phys. Lett.* **2004**, *85*, 127.
[68] Z. Xu, X. D. Bai, E. G. Wang, Z. L. Wang, *Appl. Phys. Lett.* **2005**, *87*, 163 106.
[69] I. Ozerov, private communication **2005**.
[70] W. P. Dyke, J. K. Trolan, *Phys. Rev.* **1953**, *89*, 799.
[71] W. P. Dyke, J. K. Trolan, E. E. Martin, J. P. Barbour, *Phys. Rev.* **1953**, *91*, 1043.
[72] W. W. Dolan, W. P. Dyke, J. K. Trolan, *Phys. Rev.* **1953**, *91*, 1054.

